International Journal of Pharmaceutics 395 (2010) 232–235

Contents lists available at ScienceDirect

International Journal of Pharmaceutics

journal homepage: www.elsevier.com/locate/ijpharm

Rapid communication

Is a distinctive single T_g a reliable indicator for the homogeneity of amorphous solid dispersion?

Feng Qian[a,*], Jun Huang[a], Qing Zhu[b], Raja Haddadin[a], John Gawel[a], Robert Garmise[a], Munir Hussain[a]

[a] Biopharmaceutics R&D, Bristol-Myers Squibb Company, One Squibb Drive, 105-2-1A, New Brunswick, NJ 08903, USA
[b] Department of Chemical Engineering, Purdue University, West Lafayette, IN 47907, USA

ARTICLE INFO

Article history:
Received 25 March 2010
Received in revised form 27 April 2010
Accepted 15 May 2010
Available online 24 May 2010

Keywords:
Amorphous solid dispersion
Homogeneity
T_g
Confocal Raman microscopy
Hot-melt extrusion

ABSTRACT

For an amorphous drug–polymer solid dispersion, a distinctive single T_g intermediate of the two T_g values of the two components has been widely considered as an indication of the mixing uniformity, which is critical for the stability of the amorphous drug against crystallization. In this study, two batches of amorphous solid dispersions consisting of BMS-A, a poorly water-soluble drug, and PVP-VA, were made by a twin-screw hot-melt extruder using different processing conditions. Both batches displayed an identical distinctive single T_g that is consistent with the prediction of Fox equation assuming homogeneous mixing of the two components. Neither DSC nor PXRD detected any drug crystallinity in either batch. However, the two batches exhibited different physical stability against crystallization over time. The application of a Raman mapping method showed that the drug distributed over a much wider concentration range in the less stable solid dispersion. It is therefore experimentally demonstrated that, in the characterization of amorphous solid dispersions, a distinctive single T_g may not always be a reliable indicator of homogeneity and optimal stability, and more examinations and new techniques may be required other than conventional studies.

1. Introduction

Over the past decade, amorphous drug–polymer solid dispersions have evolved into one of the major drug delivery platform technologies for the increasing amount of poorly water-soluble drugs entering into development (Serajuddin, 1999; Leuner and Dressman, 2000; Janssens and Van den, 2009). The drug is stabilized in the amorphous form when dispersed into a polymer matrix. The higher solubility of the amorphous drug compared with the crystalline counterpart, the improved material wetability, and possibly the prolonged *in vivo* super-saturation after dosing, could synergistically enhance the *in vivo* drug absorption (Hancock and Parks, 2000; Hancock, 2002).

In the development of solid dispersions, physical stability of the amorphous drug against crystallization is one of the key concerns. Depending on the drug loading, drug-polymer solubility and miscibility, and its glass transition temperature (T_g), a solid dispersion could have different thermodynamic nature and crystallization/destabilization driving forces (Qian et al., 2010). Although it is still not completely clear as how the polymer stabilizes the amorphous drug in the mixture, drug-polymer mixing homogeneity is generally accepted as one of the critical attributes that affect the stability of the solid dispersion. An inhomogeneous solid dispersion with unintended drug rich regions could lead to unexpected destabilization and bring much uncertainty for risk management.

A distinctive single T_g of the solid dispersion, which is intermediate of the T_g of the pure drug and that of the polymer, has been widely considered as a reliable proof of the homogeneity of the amorphous mixture at the molecular level (Kennedy et al., 2008; Rumondor and Taylor, 2009; Rumondor et al., 2009; Andrews et al., 2009; Tobyn et al., 2009). One recognized limitation of this approach is, the phase separation region has to be larger than ~30 nm, when DSC is used to measure the T_g (Krause and Iskander, 1977). In practice, however, little detailed experimental data is available to evaluate the limit of using the DSC method for the assessment of mixing homogeneity and physical stability of an amorphous solid dispersion.

In this communication, we demonstrate that the poor homogeneity of an amorphous mixture, even with phase separation at the scale of tens of microns, may still be undetectable by DSC. Therefore, a distinctive single T_g under this circumstance may be misleading in the assessment of physical stability of solid dispersions. The results also suggest that conventional characterizing techniques like DSC and powder X-ray diffraction (PXRD) may have their limitations in capturing the localized compositional distribution of the

* Corresponding author. Tel.: +1 732 227 6131.
E-mail address: feng.qian1@bms.com (F. Qian).

0378-5173/$ – see front matter © 2010 Elsevier B.V. All rights reserved.
doi:10.1016/j.ijpharm.2010.05.033

solid dispersion, and supplemental tools such as confocal Raman microscopy (CRM) may be promising for this purpose.

2. Materials and methods

2.1. Materials

BMS-A (molecular weight: 520; T_m: 160 °C; T_g: 45 °C) is a poorly water-soluble drug synthesized in Bristol-Myers Squibb Company. Poly(vinylpyrrolidone-co-vinylacetate) (PVP-VA) random copolymer was obtained from BASF (Ludwigshafen, Germany). HPLC grade acetone was obtained from EMD Chemicals (Bibbsons Town, NJ).

2.2. Preparation and characterization of BMS-A/PVP-VA solid dispersions

Mixture of crystalline BMS-A (40%, w/w) and PVP-VA (60%, w/w) was charged into an 8 Qt V-Blender and blended for 15 min at 12 rpm. The blend was fed at a speed of 1.5 kg/h into an 18 mm twin-screw extruder (Leistritz Corporation, Nuernberg, Germany), and the processing temperature across all heating zones was 150 °C. Two hot-melt extrudate batches, HME 1 and HME 2, were made with screw speed of 50 and 225 rpm, respectively. The resulted hot-melt extrudates were cut into cylindrical rods (~2 mm in diameter, and 10–20 cm in length). Some rods were further milled by mortar and pestle into powder, and characterized by powder X-ray diffraction (PXRD, Bruker D8 Advance Diffractometer, Bruker AXS, Inc. Madison, WI) and Differential Scanning Calorimetry (DSC, TA DSC Q1000, New Castle, DE), both at time zero and 2 months after being exposed to ambient conditions (20–25 °C, 40–60% RH). For the DSC study, ~5 mg sample was loaded into crimped aluminum pan, and heated to 180 °C at 10 °C/min.

2.3. Confocal Raman microscopy

Standard amorphous solid dispersion samples were prepared by spray drying drug–polymer acetone solutions using a Buchi B-290 mini spray dryer (Brinkmann Instruments, Westbury, NY). The spray dried standard samples were then melted on glass slides, and Raman spectra of these standard samples were collected by a Thermo Scientific (Waltham, MA, USA) confocal DXR Raman microscopy (CRM) equipped with a 532 nm laser. Background and fluorescence corrections were applied. The standard curve correlates the drug concentration to the peak height ratio of the API characteristic band (~1630 cm^{-1}) and the PVP-VA characteristic band (~1735 cm^{-1}). It was observed that these bands do not shift significantly across different drug/polymer ratios (refer to Fig. 2A).

Raman maps were acquired with the hot-melt extrudate rods without milling. For each sample, Raman spectra were collected within 4 randomly selected 800 μm × 800 μm horizontal planes that were 100–200 μm underneath the surface of the rods. The step size of Raman mapping was 20 μm on both axis (i.e., 40 sampling × 40 sampling in one plane). Raman signal was collected using a 50× dry objective and a 25 μm pinhole aperture to achieve the ~2 μm spatial resolution. The estimated size of the laser spot under this condition was 0.7 μm and the estimated spectral resolution was 9 cm^{-1}. The laser power was set to 8 mW. The compositional maps were then generated from the standard curve.

3. Results and discussion

As shown in Fig. 1A, DSC detected a single T_g at approximately 88 °C in both HME 1 and HME 2, which is intermediate of the

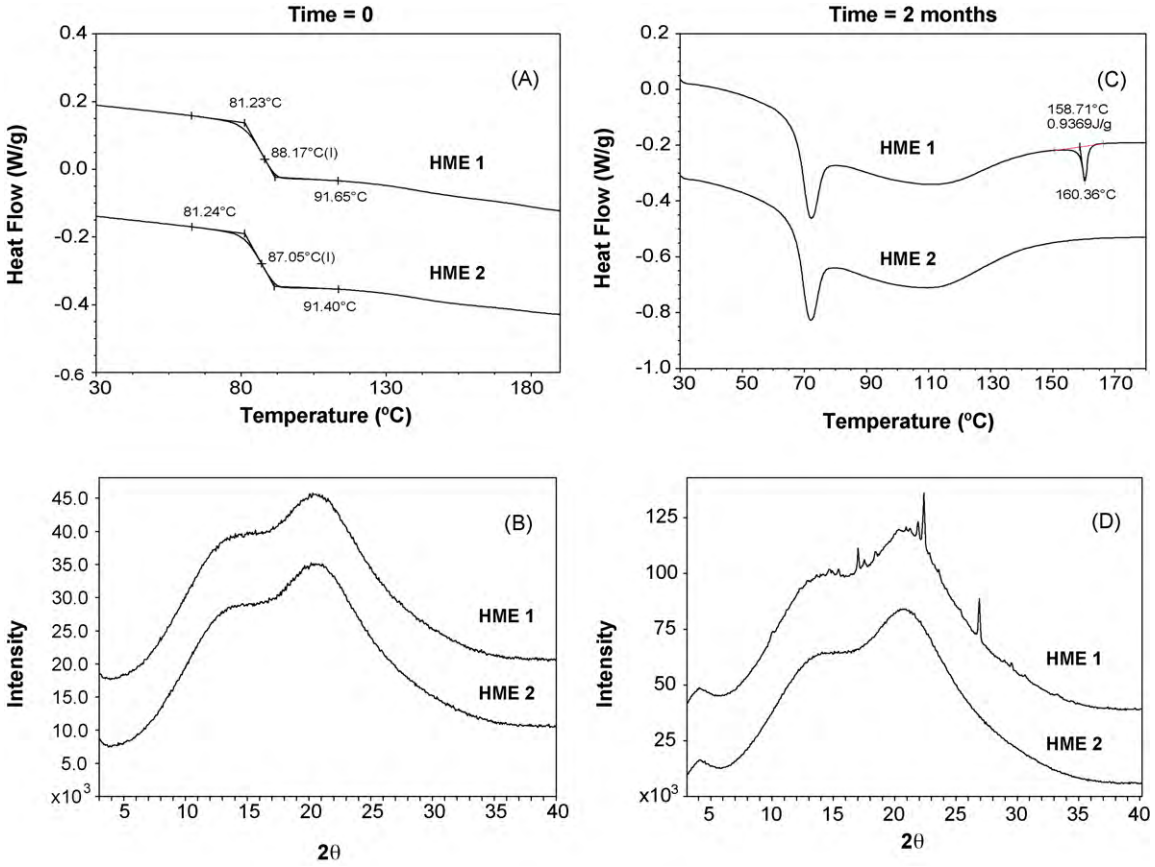

Fig. 1. DSC and PXRD results of hot-melt extruded BMS-A/PVP-VA solid dispersions, HME 1 and HME 2. (A and B) DSC and PXRD of HME 1 and HME 2 immediately after extrusion and milling; (C and D) DSC and PXRD of HME 1 and HME 2 after 2 months storage under ambient conditions (approximately 20–25 °C, 40–60% RH).

T_g of the pure amorphous API (45 °C) and that of the polymer (110 °C). This T_g value is reasonably close to the prediction of ~81 °C by the Fox equation (Fox, 1956), assuming homogenous mixing and no specific interactions between the two amorphous components. Melting of crystalline API (~160 °C) was not detected in either of HME 1 or HME 2. PXRD spectra (Fig. 1B) of HME 1 and HME 2 appear to be identical too, with no crystalline API detected. Based on these data, a quick conclusion one might have drawn is, HME 1 and HME 2 are homogenously mixed and practically identical.

Surprisingly, HME 1 and HME 2 demonstrated different physical stability. When stored under ambient conditions for 2 months, an endothermic event at ~160 °C, presumably due to the melting of the crystalline API, was detected in HME 1 (Fig. 1C). The existence of API crystals in HME 1 was also confirmed by PXRD (Fig. 1D). However, neither DSC nor PXRD detected any API crystals in HME 2. The decrease in T_g of both HME 1 and HME 2 from the initial ~88 °C to ~70 °C could be due to the ~2% (w/w) moisture sorption under the ambient environment, while the initial materials were practically dry immediately after hot melt extrusion (confirmed by thermal gravity analysis). This is fairly consistent with the Fox equation prediction using a reported water T_g value of −108 °C (Velikov et al., 2001). HME 1 and HME 2 also relaxed over the 2-month period (i.e., enthalpy relaxation) (Hancock et al., 1995) giving rise to the endothermic peaks at T_g (Fig. 1C).

To further explore the difference of physical stability between HME 1 and HME 2, we applied CRM to study the localized compositional distribution/fluctuation of the two solid dispersions as DSC and PXRD only probe the bulk properties.

For this purpose, a standard curve was constructed to correlate the composition of the dispersion (i.e., drug/polymer mass ratio) to the Raman signal (i.e., intensity ratio of the API characteristic band and the polymer characteristic band) as shown in Fig. 2. A linearity of R^2 = 0.998 was obtained with high reproducibility when the drug/polymer mass ratio was < 1.5 (i.e., <60% (w/w) API in the solid dispersion). When the mass ratio was >1.5 (i.e., drug loading >60%, w/w), accurate quantification of drug concentration became challenging due to the weak intensity of the PVP-VA characteristic band. Similarly, when the mass ratio was <0.25 (i.e., drug loading <20%, w/w), difficulty arises due to the decreasing intensity of BMS-A band.

Using the standard curve, Raman images of the compositional distributions of HME 1 and HME 2 were obtained and the representative ones are shown in Fig. 3A and B. Evidently, HME 1 has much poorer homogeneity compared with HME 2. Although 40% (w/w) drug concentration is targeted, the value was much higher than 50% (w/w) (Fig. 3C) in some regions of HME 1 (i.e., the red area in Fig. 3A), while the drug distributed fairly uniformly in HME 2 (Fig. 3B) with a narrow fluctuation around 40% (w/w) (Fig. 3D). The higher local drug concentration observed in HME 1 may facilitate the crystallization of the API, presumably due to the lower T_g resulted from the higher drug/polymer mass ratio; and possibly, the reduced drug–polymer interaction, although further studies are required for the verification. On the other hand, the broad compositional distribution observed in HME 1 may not necessarily lead to a DSC trace with multiple T_gs. The continuous compositional spreading of HME 1 may result in the "stacking" of a series of continuously varying T_g values contributed by numerous amorphous zones. Collectively, an apparent single T_g, similar to the theoretical value, could be obtained from a weight fractioned averaging. The "distinctive single T_g" in this situation is just apparent for the bulk property and could lead to a misleading conclusion that the system is homogenously mixed. Instead, CRM was shown in this case to be a useful supplemental technique that provides localized compositional information that are distinctive from the bulk characterization. Other analytical tools such as solid state NMR (Berendt et al., 2006; Aso et al., 2007) and pair distribution function analysis (Newman et al., 2008) may also find their applications in the characterization of amorphous solid dispersions if used properly.

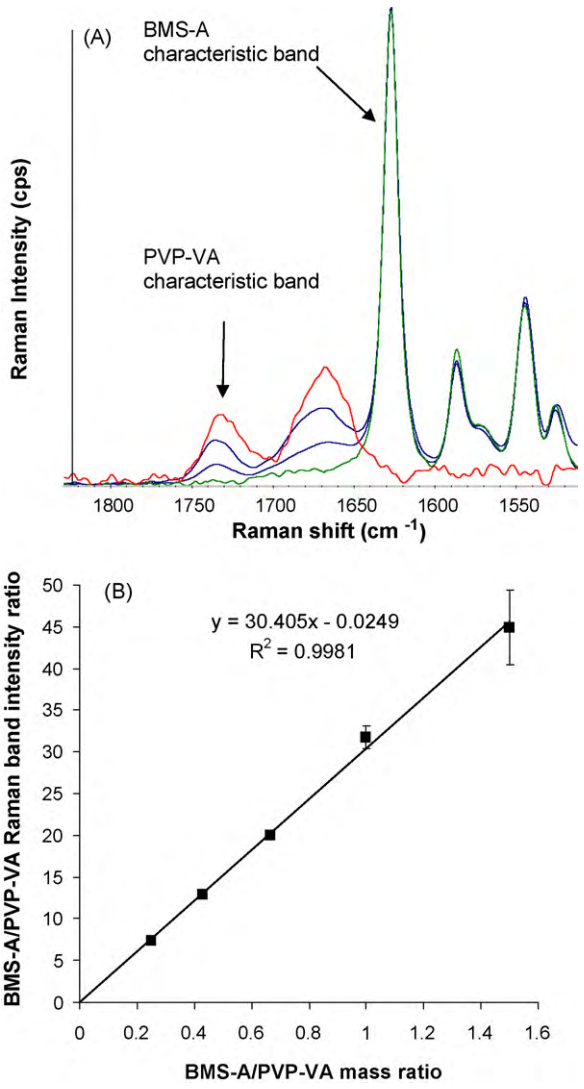

Fig. 2. (A) Raman spectra of BMS-A, PVP-VA and BMS-A/PVP-VA dispersions in the range of interest (from top to bottom: PVP-VA; 30/70 and 50/50 (w/w) BMS-A/PVP-VA dispersions; and amorphous BMS-A). A BMS-A characteristic band and a PVP-VA characteristic band were selected for quantitative calculation of BMS-A/PVP-VA mass ratio. The intensity of BMS-A characteristic bands of all materials was normalized for easy comparison. (B) The calibration curve correlating the BMS-A/PVP-VA mass ratio and the intensity ratio of BMS-A vs. PVP-VA characteristic bands. Standard samples of different BMS-A/PVP-VA ratio were prepared by spray drying, and average values from 3 measurements were used to construct the standard curve.

Different screw speeds used in the hot-melt extrusion process seemed to be important for the mixing homogeneity of HME 1 and HME 2. A slow speed of 50 rpm apparently failed to achieve satisfactory mixing in HME 1 while a much faster speed of 225 rpm produced much better uniformity as in HME 2. A comprehensive correlation between the processing conditions of hot-melt extrusion process (screw configuration, screw speed, temperature at different zones, material feeding rate, etc.) and the solid dispersion homogeneity requires further planning and execution of a better-controlled study and will be the subject of a future report.

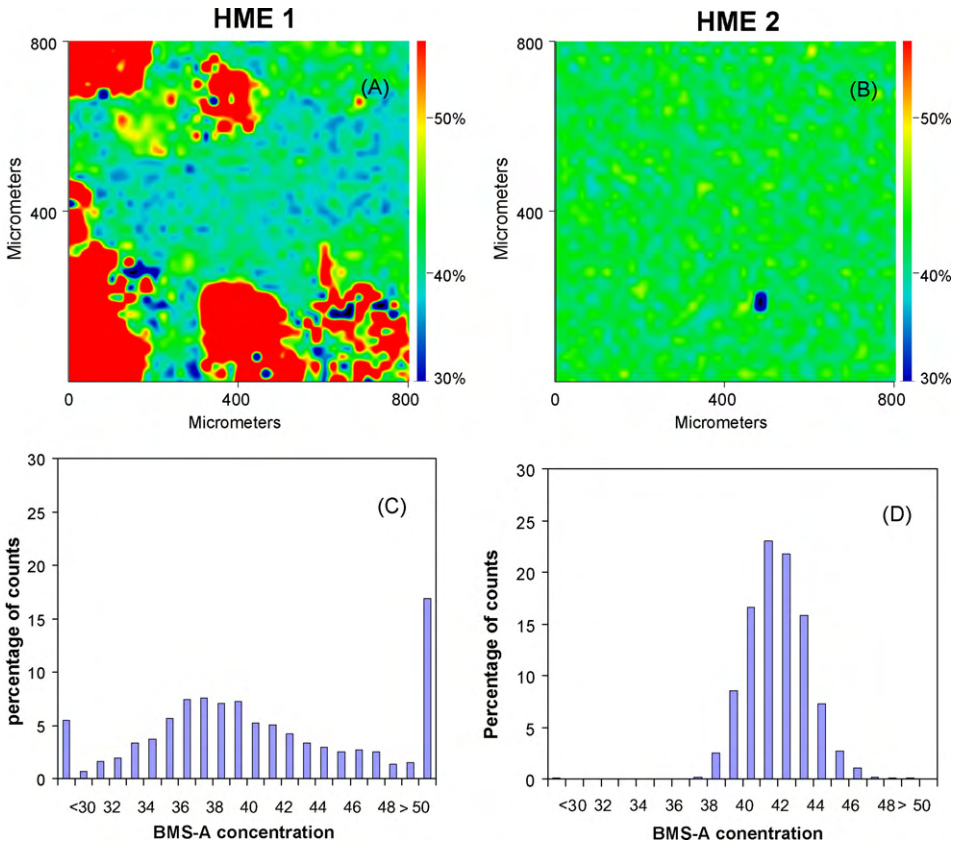

Fig. 3. (A and B) Representative compositional Raman images of HME 1 and HME 2, respectively. Red color represents higher concentration of BMS-A. The size of each Raman map is 800 μm × 800 μm and 1600 (40 × 40) Raman spectra were collected to construct each image. (C and D) Drug concentration histograms of HME 1 and HME 2, respectively, constructed by fractionizing the 1600 Raman sampling spots of each image into different ranges of drug concentration (% w/w). (For interpretation of the references to color in this figure legend, the reader is referred to the web version of the article.)

4. Conclusion

We studied the solid dispersions prepared by hot-melt extrusion under different processing conditions using DSC, PXRD and CRM. It was demonstrated experimentally that a distinctive single T_g by DSC may be misleading in the indication of mixing homogeneity of amorphous solid dispersions and therefore not sufficient to provide all the necessary information for stability assessment. Other supplemental tools such as confocal Raman microscopy (CRM) may be promising in capturing the localized compositional distribution of solid dispersions and better correlating the physical stability to processing conditions under this circumstance.

References

Andrews, G.P., Abudiak, O.A., Jones, D.S., 2010. Physicochemical characterization of hot melt extruded bicalutamide–polyvinylpyrrolidone solid dispersions. J. Pharm. Sci. 99 (March (3)), 1322–1335.

Aso, Y., Yoshioka, S., Miyazaki, T., Kawanishi, T., Tanaka, K., Kitamura, S., Takakura, A., Hayashi, T., Muranushi, N., 2007. Miscibility of nifedipine and hydrophilic polymers as measured by (1)H-NMR spin-lattice relaxation. Chem. Pharm. Bull. (Tokyo) 55, 1227–1231.

Berendt, R.T., Sperger, D.M., Munson, E.J., Isbester, P.K., 2006. Solid-state NMR spectroscopy in pharmaceutical research and analysis. TrAC, Trends Anal. Chem. 25, 977–984.

Fox, T.G., 1956. Influence of diluent and of copolymer composition on the glass transition temperature of a polymer system. Bull. Am. Phys. Soc. 1, 123.

Hancock, B.C., 2002. Disordered drug delivery: destiny, dynamics and the Deborah number. J. Pharm. Pharmacol. 54, 737–746.

Hancock, B.C., Parks, M., 2000. What is the true solubility advantage for amorphous pharmaceuticals? Pharm. Res. 17, 397–404.

Hancock, B.C., Shamblin, S.L., Zografi, G., 1995. Molecular mobility of amorphous pharmaceutical solids below their glass transition temperatures. Pharm. Res. 12, 799–806.

Janssens, S., Van den, M.G., 2009. Review: physical chemistry of solid dispersions. J. Pharm. Pharmacol. 61, 1571–1586.

Kennedy, M., Hu, J., Gao, P., Li, L., Ali-Reynolds, A., Chal, B., Gupta, V., Ma, C., Mahajan, N., Akrami, A., Surapaneni, S., 2008. Enhanced bioavailability of a poorly soluble VR1 antagonist using an amorphous solid dispersion approach: a case study. Mol. Pharmacol. 5, 981–993.

Krause, S., Iskander, M., 1977. In: Klempner, D., Frisch, K. (Eds.), Phase Separation in Styrene-a-Methyl Styrene Block Copolymers, pp. 231–243.

Leuner, C., Dressman, J., 2000. Improving drug solubility for oral delivery using solid dispersions. Eur. J. Pharm. Biopharm. 50, 47–60.

Newman, A., Engers, D., Bates, S., Ivanisevic, I., Kelly, R.C., Zografi, G., 2008. Characterization of amorphous API:polymer mixtures using x-ray powder diffraction. J. Pharm. Sci. 97, 4840–4856.

Qian, F., Huang, J., Hussain, M.A., 2010. Drug–polymer solubility and miscibility: stability consideration and practical challenges in amorphous solid dispersion development. J. Pharm. Sci. 99 (July (7)), 2941–2947.

Rumondor, A., Taylor, L.S., 2010. Effects of polymer hygroscopicity on the phase behavior of amorphous solid dispersions in the presence of moisture. Mol. Pharmaceutics 7 (2), 477–490.

Rumondor, A.C., Marsac, P.J., Stanford, L.A., Taylor, L.S., 2009. Phase behavior of poly(vinylpyrrolidone) containing amorphous solid dispersions in the presence of moisture. Mol. Pharmacol. 6, 1492–1505.

Serajuddin, A.T., 1999. Solid dispersion of poorly water-soluble drugs: early promises, subsequent problems, and recent breakthroughs. J. Pharm. Sci. 88, 1058–1066.

Tobyn, M., Brown, J., Dennis, A.B., Fakes, M., Gao, Q., Gamble, J., Khimyak, Y.Z., McGeorge, G., Patel, C., Sinclair, W., Timmins, P., Yin, S., 2009. Amorphous drug-PVP dispersions: application of theoretical, thermal and spectroscopic analytical techniques to the study of a molecule with intermolecular bonds in both the crystalline and pure amorphous state. J. Pharm. Sci. 98, 3456–3468.

Velikov, V., Borick, S., Angell, C., 2001. The glass transition of water, based on hyperquenching. Science 294, 2335–2338.